An Indoor 3D Positioning Method Using Terrain Feature Matching for PDR Error Calibration

Xintong Chen , Yuxin Xie , Zihan Zhou , Yingying He , Qianli Wang , Zhuming Chen *

Posted Date: 23 February 2024

doi: 10.20944/preprints202402.1364.v1

Keywords: indoor three-dimensional positioning; PDR; terrain features; feature matching; pattern recognition

Article

An Indoor 3D Positioning Method Using Terrain Feature Matching for PDR Error Calibration

Xintong Chen [1], Yuxin Xie [1], Zihan Zhou [1], Yingying He [1], Qianli Wang [2] and Zhuming Chen [1,*]

[1] Yangtze Delta Region Institute (Quzhou), University of Electronic Science and Technology of China, Quzhou, China
[2] The School of Information Science and Technology, Southwest Jiaotong University, Chengdu, China
* Correspondence: zmchen@uestc.edu.cn

Abstract: Pedestrian Dead Reckoning (PDR) is a promising algorithm for indoor positioning. However, the accuracy of PDR degrades due to the accumulated error, especially in multi-floor buildings. This paper introduces a three-dimensional (3D) positioning method based on terrain feature matching to reduce the influence of accumulated error in multi-floor scene. The proposed method involves two steps: motion pattern recognition and position matching calibration. The motion pattern recognition aims to detect different motion states, i.e., taking the stairs or horizontal walking, from the streaming data. Then, stair entrances and corridor corners are matched with transition points of motion states and pedestrian turning points, respectively. After matching, calibration is performed to eliminate the accumulated errors. By carrying out experiments on a two-floor closed-loop path with a walking distance about 145 m, it is shown that this method can effectively reduce the accumulated error of PDR, achieving accurate 3D positioning. The average error is reduced from 6.60 m to 1.83 m.

Keywords: indoor three-dimensional positioning; PDR; terrain features; feature matching; pattern recognition

1. Introduction

Indoor positioning technology is of great significance for location-based services (LBS) and boasts a wide range of applications in our daily lives [1], such as emergency rescue and hospital navigation [2–4]. In recent years, with the miniaturization and integration of sensors, Inertial navigation positioning technology based on Inertial Measurement Unit (IMU) has been frequently adopted to indoor pedestrian tracking and navigation [5,6]. One of the main implementation methods is Pedestrian Dead Reckoning (PDR) algorithm [7,8]. However, it inevitably incurs cumulative positioning errors that cannot be mitigated over time. There are two solutions to this problem: one is infrastructure-based method, and the other is infrastructure-free method.

The infrastructure-based methods combine UWB [9], WiFi [10], Bluetooth, and other technologies. However, these technologies rely on supporting infrastructure, which entails time-consuming, laborious, and costly large-scale facility installations [11]. Meanwhile, due to the constraints of indoor terrain, the signal is significantly interfered with the multipath effect [12]. Therefore, the infrastructure-based PDR calibration algorithm can hardly be applicated to constrained terrain scene.

The infrastructure-free PDR calibration method reduces error through algorithmic process. A representative method is zero-velocity update algorithm (ZUPT) [13,14]. However, it is inapplicable for practical conditions since it is generally suited for foot-based dead reckoning systems, which require specially designed shoes or insoles to secure the inertial sensor. Tying inertial sensors to the waist can result in better performance compared to placing it on the foot [15,16]. Li et al. [17] designed a magnetic matching-assisted indoor positioning system based on waist-mounted sensor array. However, the performance of this method will decrease due to the magnetic interference generated by metal objects in modern architecture. In the case of avoiding external interference, Shi et al. [18]

 doi:10.20944/preprints202402.1364.v1

proposed a PF-SLAM indoor pedestrian location algorithm based on a feature point map without prior knowledge of the map. However, the accuracy of the constructed feature points depends on the amount of data and the accuracy of device, which bring high cost and instability for positioning. Note that only the building structure will remain constant, and it is presented on the map. The method of setting landmarks on the map for matching can help to calibrate the positioning error [19]. Ghaoui et al. [20] designed a landmark matching system based on a PDR and particle filter (PF), achieving a high-precision indoor positioning result. Although these methods can achieve better performance in 2D positioning, they cannot achieve 3D positioning, which has a wider range of application scenarios.

Yang et al. [21] extended the indoor positioning problem to three dimensions by combining with multiple sensors. Zhao et al. [22] combined inertial sensing devices with barometer for 3D positioning. They effectively eliminated the accumulated altitude estimation error caused by the inherent drift of IMU sensors through complementary filters and error compensation algorithms. However, the error of above methods is essentially derived from the influence of the environment. In order to avoid the influence of the external environment, Xie et al. [23] proposed a foot-mounted pedestrian navigation system with IMU. The experiment results show its high accuracy in 2D positioning and altitude estimation. The method they proposed relies on the pre-obtained motion pattern of a pedestrian, that is, the zero velocity detection method and lateral velocity restriction method are applied when a pedestrian walks horizontally in 2D plane, and the stair step height correction method is applied when a pedestrian takes stairs. Under the condition of continuous 3D positioning, the motion pattern of a pedestrian will change, thus introducing extra accumulated error which is hard to be eliminated by the previous methods.

Fortunately, the change of motion pattern of people also provides extra information of their position in the building. Therefore, in this paper, a 3D positioning scheme is proposed to obtain the positional information of a pedestrian with the aid of motion pattern recognition. Based on landmark matching method mentioned above, we note that indoor corners contain clear location and direction information, which can be used as landmarks for identifying turns in behavior [24]. Therefore, we could use the terrain features of the building, i.e., indoor stair entrances and the corners of the corridor to calibrate the error, achieving accurate 3D positioning. The Terrain Feature Matching Calibration (TFMC) method is as follows: (1) The time domain feature information of the accelerometer is extracted, then the path motion pattern is identified by pattern feature matching, and the altitude information of the pedestrian is calculated according to the motion pattern. (2) Combining the PDR algorithm with the altitude information of the pedestrian, the walking paths of the pedestrian is fitted. For the paths of taking the stairs, the stair entrances are matched with the changed points of horizontal walking to the stairs. The calibration of these paths is achieved through the coordinate calibration. For the paths of horizontal walking, the corners of the corridor are matched with the turning points of pedestrian. The calibration of these paths is achieved through the calibration of the coordinate, step length and yaw. The main contribution of this method is that it can effectively reduce PDR error, and thereby accurately calibrate pedestrian 3D walking trajectory without any devices except IMU.

The rest of this paper is structured as follows. First, Section 2 discusses some related work in the paper. Section 3 introduces the Terrain Feature Matching Calibration (TFMC) method under indoor constrained terrain. Section 4 conducts experimental verification and result analysis. Section 5 summarizes the full text.

2. Related Works

2.1. Altitude Estimation

In indoor 3D positioning, the altitude information of a pedestrian is typically obtained through the second-order integration of vertical acceleration data. In addition, some researchers use pattern recognition to assist in height estimation. By extracting time-domain features from the sensor as a feature vector, Xia et al. [25] designed an adaptive network-based fuzzy inference system (ANFIS) to identify vertical motion patterns and estimate altitude. Since the algorithm's solution depends on

 doi:10.20944/preprints202402.1364.v1

zero-speed information, it cannot be directly applied to altitude estimation in the scenario of this paper. After extracting the features for motion recognition from the inertial sensor, feature matching is performed by measuring the similarity between features to identify the pedestrian's motion pattern [26]. Template matching is a general method for determining the similarity between feature vectors [27].

Inspired by above methods, this paper selects an accelerometer time-domain feature quantity with significant discrimination and applies the KNN (K-Nearest Neighbors) algorithm to measure the feature similarity to identify motion patterns. Based on the terrain information that corresponds with the motion pattern, the altitude of the pedestrian can be calculated.

2.2. PDR Error Calibration with Feature Matching

For the horizontal walking pattern with no changes in altitude, the horizontal walking path is fitted using the PDR algorithm. It includes three steps: step detection, step length estimation, and yaw estimation. These steps are used to obtain the step length and direction of travel from the starting position in order to calculate the pedestrian's next moment location [28], as Equation (1) shows:

$$\begin{cases} x_{i+1} = x_i + SL_i sin\theta_i \\ y_{i+1} = y_i + SL_i cos\theta_i \end{cases} \quad (1)$$

where SL_i and θ_i represent the step length and the walking direction, and the ith step (x_i, y_i) is the current position. For step detection, pedestrian walking posture can be detected by setting the peak acceleration threshold and the peak interval threshold to achieve accurate step counting [29]. For step length estimation, Weinberg considered that the step length is proportional to the difference between peak and valley accelerations. He then proposed a famous step length estimation model [30]. The heading information is obtained from the second-order integration of the gyroscope's output angular velocity data. Based on the above work, the PDR algorithm is used to fit the pedestrian path that needs to be calibrated.

When performing terrain feature matching to calibrate PDR error, some indicators are used to measure the similarity between pedestrian trajectories and terrain features, i.e., the Euclidean distance [20], the correlation coefficient [31]. However, due to the cumulative positioning error, using a single indicator for matching has a high mismatch rate.

Therefore, the above indicators are combined in our method. Taking the correlation coefficient between feature path segments and the Euclidean distance of feature points as measurement indicators, the Terrain Feature Matching Calibration (TFMC) method is proposed to calibrate the indoor PDR error based on engineering drawings alone.

3. TFMC Method

3.1. Method Overview

The two main terrain features in a building are stairs and flat ground, which can be characterized by the motion patterns of pedestrians. Combined with the vertical direction of pedestrian movement, the motion patterns of pedestrians indoors mainly include horizontal walking, going upstairs, and going downstairs. The motion pattern of the pedestrian can be reflected in the time-domain characteristics of an accelerometer. The KNN algorithm is used for feature matching to identify the motion pattern and infer terrain information. Based on the result of motion pattern recognition, the inertial sensor measurement data is divided into two categories, taking stairs and horizontal walking. The altitude of the pedestrian is calculated with terrain information, and the stair entrance is judged. Subsequently, the stair path is fitted with pedestrian altitude reckoning, and the horizontal path is fitted with the PDR algorithm.

For PDR error calibration, terrain feature points are selected for matching. The corners of the corridor and the stair entrance are unique terrain features indoors. Due to the limitations of width of the corridor, the angle of rotation when pedestrians walk towards the corner is restricted within a specific range by the terrain. The stair entrance is where pedestrians begin their journey on the stair

 doi:10.20944/preprints202402.1364.v1

path, and it marks a change in altitude for them as well. Therefore, this paper selects the corners of the corridor and the stair entrance as terrain feature points to calibrate the PDR error. According to engineering drawings, the two-dimensional coordinates of all indoor terrain feature points are obtained.

For the stair path, a position matching calibration method is proposed. The stair entrance where pedestrian enters is considered as the path feature point, and the building stair entrance is considered as the terrain feature point. Combined with the Euclidean distance between the two feature points, the path feature points are matched with the terrain feature points. After the terrain matching, the coordinates of the path feature points are calibrated. For the horizontal path, an extended position matching calibration method is proposed. The position where the pedestrian turns is considered to be a path feature point, while the corner of a corridor is deemed to be a terrain feature point. Combined with the linear correlation coefficient between the feature path segment to be calibrated and the standard feature path segment, as well as the Euclidean distance of their respective feature points, the path feature points are matched with terrain feature points. Subsequently, the coordinates of the path feature points are calibrated. The step length and yaw angle are further calibrated to complete the path calibration. Finally, the calibrated path is spliced according to the time sequence to reconstruct the path, and the calibrated three-dimensional path is obtained.

Figure 1 gives an overview of the proposed TFMC method.

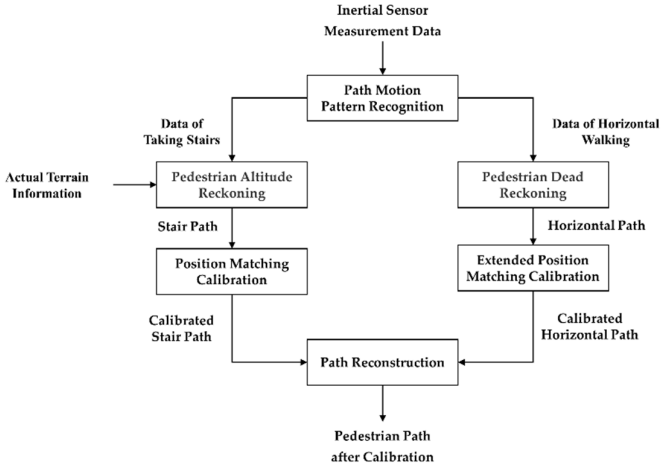

Figure 1. TFMC method flow.

3.2. Path Motion Pattern Recognition

The interquartile range (IQR), is used to measure the intensity of signal change. The value of IQR increases with the increase of signal change intensity. The length of the series is set as 100, and the data of the series are arranged in descending order. The calculation formula of the IQR is as follows:

$$Q_{IQR} = Q_3 - Q_1 \tag{2}$$

where Q_3 and Q_1 are the median values of the first 50 and the last 50 data, respectively.

In indoor terrain, the amplitude of movement for pedestrians going upstairs and walking horizontally is significantly smaller than when going downstairs. This is reflected in the intensity of linear acceleration changes in the vertical direction. Therefore, the motion pattern can be characterized by the interquartile range (IQR) of the linear acceleration. And the linear acceleration in the vertical direction of the pedestrian can be obtained through inertial sensors.

It can be seen from the indoor building structure that when a pedestrian walks in a constrained terrain, the pedestrian will turn significantly at the corner of the corridor to enter the next constrained terrain area. A pedestrian will first pass through a corner of the corridor before reaching the stair

 doi:10.20944/preprints202402.1364.v1

entrance. Therefore, the turning time point can be used to segment the IQR data, and the complex walking process of a pedestrian can be divided into several parts containing single motion patterns. With the sliding window detection method, if the window continuously detects coordinate points that meet the threshold conditions, then the last coordinate point is regarded as a corridor turning point. The segmentation of IQR is shown in Figure 2.

According to the figure, the pedestrian walking process is divided into nine segments. These segments are roughly categorized based on the size of their IQR values. The cumulative probability distribution curve is shown in Figure 3.

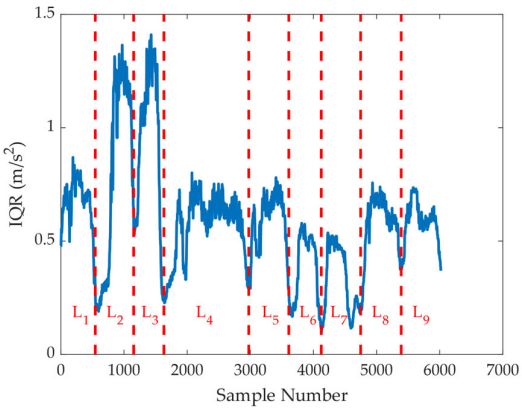

Figure 2. The sub-IQR after data segmentation.

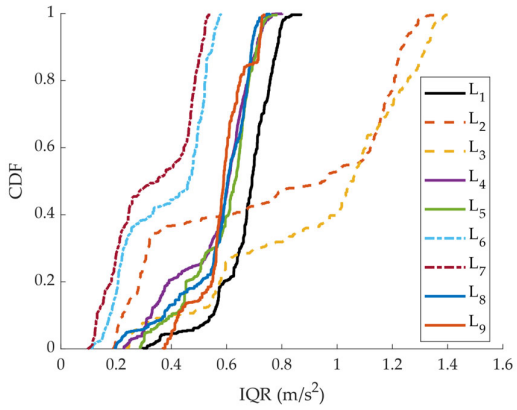

Figure 3. Segmented IQR cumulative probability distribution.

The mean and standard deviation of the IQR data are selected as the characteristic variables for matching, and standard deviation is computed by:

$$\mathrm{STD} = \sqrt{\frac{1}{N-1}\sum_{i=1}^{N}(\omega_i - \bar{\omega})^2} \tag{3}$$

where ω_i is the sample data, $\bar{\omega}$ is the sample average, and N denotes the sample number. As depicted in Figure 4, acceleration data for the three motion patterns were collected utilizing an inertial sensor, comprising 100 groups for each pattern.

 doi:10.20944/preprints202402.1364.v1

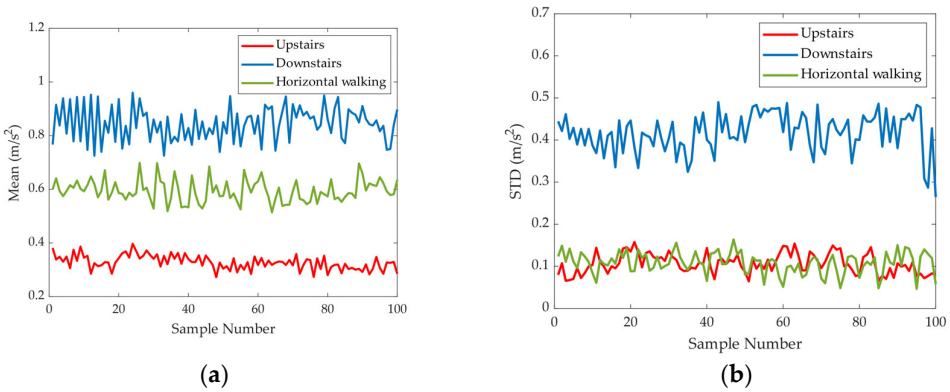

Figure 4. Comparison of mean and standard deviation of IQR under different motion patterns; (a) mean; (b) standard deviation.

Analysis of the time-domain characteristics of the IQR shows a distinct ascending trend for mean values when comparing the patterns of going upstairs, walking horizontally, and going downstairs. Additionally, the standard deviation of going downstairs is significantly larger than that of walking horizontally or going upstairs. The mean and standard deviation of the IQR are composed of pattern feature points that can be used to characterize the motion pattern.

The KNN algorithm is used for classification. Taking the mean as the x-axis and the standard deviation as the y-axis, a two-dimensional pattern feature scatter plot is generated. As shown in Figure 5, in this feature space composed of two characteristic variables, the feature points of the three motion patterns are widely dispersed, which means significant distinguishability.

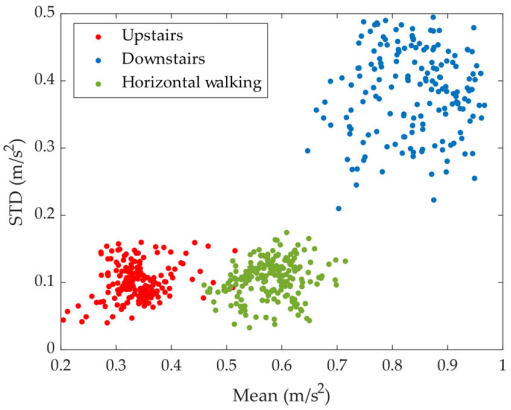

Figure 5. Two-dimensional pattern feature scatter plot of sample data.

The sample data set is randomly divided into a training set and a test set at a ratio of 7:3. The training set represents known motion patterns, while the test set represents unknown motion patterns. According to the distance criterion, the K closest training set data points are selected based on the Euclidean distance of the test set. According to the majority voting scheme, the motion pattern represented by the test set data is matched with the most common category among the K nearest neighbor samples. After five repetitions, the pattern matching accuracy for the test set is shown in Table 1.

Table 1. Test set data pattern matching results.

Motion pattern	Pattern matching results			
	Upstairs	Horizontal walking	Downstairs	Accuracy

 doi:10.20944/preprints202402.1364.v1

Upstairs	364	7	0	98.11%
Horizontal walking	5	520	0	99.05%
Downstairs	0	1	388	99.74%

According to the test results, the matching accuracy of the KNN algorithm for the three pedestrian motion patterns is higher than 98%. The comprehensive matching accuracy is 98.99%, which indicates high accuracy for the classification and recognition of motion patterns.

In the actual scene, after passing the corner of the corridor, the pedestrian will walk a distance before reaching the stair and get into either the going upstairs or going downstairs pattern. Dividing the motion pattern only based on the turning time point will result in losing some data from the horizontal walking section, which may affect the fitting and calibration of the path. Therefore, it is necessary to estimate the walking time of the pedestrian on the transition section from the corner of the corridor to the stair entrance. The time node for pattern changes is then adjusted. The straight distance D from the corner of the corridor to the stair entrance can be obtained from engineering drawings. The average speed of the pedestrian on the horizontal path that has been fitted with PDR can be calculated. The calculation formula is as follows:

$$\bar{v} = \frac{\sum_{i=1}^{n} SL_i}{T} \tag{4}$$

where SL_i is the step length of each step, and T is the total walking time.

By dividing the distance D by the average speed, we can obtain an estimate of the walking time τ for the pedestrian transition section. According to the transition time, the data of pedestrians' walking transitions are divided into horizontal sections. The change of the motion pattern occurs at the moment when the pedestrian enters or exits the stair.

Considering the terrain feature information, the upstairs pattern and downstairs pattern correspond to the stair path, while the horizontal walking pattern corresponds to the horizontal path.

3.3. Position Matching Calibration Based on Stair Path

The Pedestrian will have a short horizontal walking pattern with turns at the half-story height of the building, which will be regarded as turning feature points. Therefore, a one-floor ascending process is decomposed into two parts, and a similar situation is applied to the descending process. The number of continuous upstairs or downstairs segments identified by pattern feature matching, combined with the terrain features inside the building, can be used to derive the number of floors upstairs or downstairs, and the altitude information can be obtained.

As a simple connection passage between floors, a stair is a strong constraint that only serves to facilitate changes in altitude. Therefore, it suffices to detect the time when a pedestrian enters or exits the stair, which represents the time motion pattern changes. The information of altitude change of the pedestrian can be obtained. And the ending point of the horizontal path with transition section data fitted by PDR is set as the starting point for the adjacent stair path, which is the stair entrance position. Combined with the altitude change information, the stair path is obtained, and the complete pedestrian path is fitted.

For the stair path, a position matching calibration method is proposed. The stair entrance where pedestrian enters is regarded as the path feature point to form the set M, and the stair entrance of the building is regarded as the terrain feature point to form the set N. The Euclidean distance between all the feature points of the set M and the set N is calculated in turn. The calculation formula is:

$$\mathrm{d}(M_i, N_k) = \sqrt{(x_i - x_k')^2 + (y_i - y_k')^2 + (z_i - z_k')^2}\,, i, k = 1,2,\cdots\cdots, n \tag{5}$$

where (x_i, y_i, z_i) is the coordinate of the path feature point, (x_k, y_k, z_k) is the coordinate of the terrain feature point.

Having matched the nearest path feature point with the corresponding terrain feature point, the coordinates of the path feature points undergo calibration using those of their respective terrain feature points. This process accomplishes the coordinate calibration. Due to the long Euclidean

 doi:10.20944/preprints202402.1364.v1

distance between different stair entrances, the method based on distance matching has a high fault tolerance rate.

3.4. Extended Position Matching Calibration Based on Horizontal Path

For the horizontal path, due to the close distance between the corner feature points, relying solely on Euclidean distance matching will result in a higher mismatch rate. Therefore, an extended position matching calibration method is proposed.

The two-dimensional coordinates of the feature path segment to be calibrated, where the feature points of the path are located, are extracted to form a set P. The two-dimensional coordinates of the standard feature path segment, where the terrain features are located, are extracted to form a set Q as part of the standard path library. The schematic diagram of the path segments is shown in Figure 6.

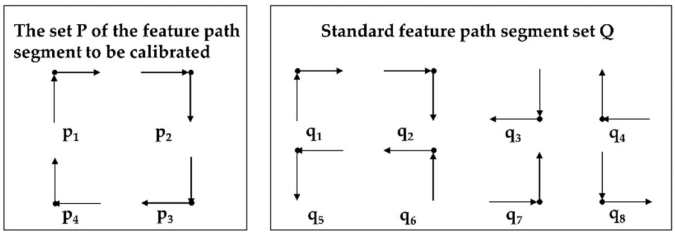

Figure 6. A schematic diagram of the set of feature path segments to be calibrated and standard feature path segments.

The abscissa of each point in the feature path segment to be calibrated constitutes the variable PX, and the ordinate constitutes the variable PY. The abscissa of the points in each standard feature path segment constitutes the variable QX, and the ordinate constitutes the variable QY. The linear correlation coefficients ρ_{PXQX} and ρ_{PYQY} between the feature path segment to be calibrated and the standard feature path segment are calculated. The calculation formula is:

$$\rho_{PXQX} = \frac{Cov(PX, QX)}{\sigma_{PX}\sigma_{QX}}, \rho_{PYQY} = \frac{Cov(PY, QY)}{\sigma_{PY}\sigma_{QY}} \tag{6}$$

where $Cov(PX, QX)$ is the covariance between the variables PX and QX, and σ_{PX}, σ_{PY}, σ_{QX}, σ_{QY} are the standard deviations of the variables PX, PY, QX, QY respectively. When the linear correlation coefficient is greater than 0.8, it is judged as a very strong positive correlation, meeting the matching conditions. The corresponding feature points of the terrain feature points and the path feature points are matched. Otherwise, no matching is performed.

If the segments in sets P and Q cannot achieve a one-to-one match, the Euclidean distance between the path feature points and the terrain feature points in the remaining path segments is calculated as follows:

$$\mathrm{d}(P_i, Q_k) = \sqrt{(x_i - x_k')^2 + (y_i - y_k')^2},\ i, k = 1,2,\cdots\cdots,n \tag{7}$$

where (x_i, y_i) is the coordinate of the path feature point, and (x_k', y_k') is the coordinate of the terrain feature point. The nearest path feature point is matched with the terrain feature point.

After feature point matching, coordinates of the path feature points are calibrated to the coordinates of the matching terrain feature points. Additionally, the step length calibration and yaw calibration can also be performed based on the feature point information at the corner of the corridor.

Concerning step length, when estimating PDR step length, the constructed step length estimation model may have deviation. Therefore, it is necessary to perform personalized step length estimation for different users through off-line calibration or external information [32]. Since the pedestrian's motion pattern is relatively stable during horizontal walking, the average step length $\overline{SL}$

 doi:10.20944/preprints202402.1364.v1

can be used to replace the step length of each step between two adjacent feature points. The average step length calculation formula is as follows:

$$\overline{SL} = S/N \tag{8}$$

where S is the distance between two adjacent path feature points, as the reference distance of pedestrian walking, and N is the number of steps between two adjacent path feature points.

For yaw calibration, the error in the yaw angle will accumulate over time. By matching the feature points, the yaw information corresponding to the terrain feature points can be used as a reliable direction for calibrating the original yaw angle. The calibration process is illustrated in Figure 7.

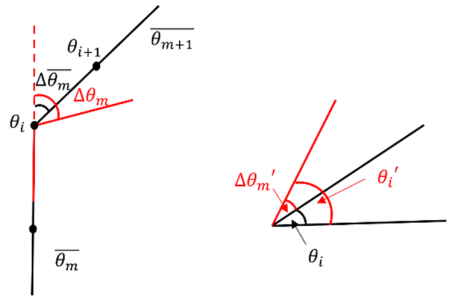

Figure 7. Yaw angle calibration diagram.

For the horizontal path divided by the turning point, the difference $\Delta\overline{\theta_m}$ between the average yaw angle of the previous horizontal path and the current horizontal path is calculated. And the yaw angle of the current horizontal path is calibrated by the terrain corner angle $\Delta\theta_m$ corresponding to the turning point. The calculation formula is :

$$\Delta\theta_m{}' = \Delta\theta_m - \Delta\overline{\theta_m} \tag{9}$$

where $\Delta\theta_m{}'$ is the calibration value of the average yaw angle of the path. The yaw angle of the current path is calibrated to:

$$\theta_i{}' = \theta_i + \Delta\theta_m{}' \tag{10}$$

where θ_i represents the yaw angle corresponding to each step of the current path. The calibrated yaw angle is averaged to update the average heading angle $\overline{\theta_{m+1}}$ of the current path. According to the order of the pedestrian passing through the corner of the corridor, above steps are carried out in turn to complete the yaw calibration.

After completing the pedestrian path calibration, the horizontal path is connected with the stair path in chronological order to reconstruct a complete 3D pedestrian path.

4. Experiments

Experiments were conducted in buildings featuring stairs and corner corridors. The architectural layout of the building is depicted in Figure 8(a). As illustrated in Figure 8(b), tester wore the inertial sensor on their waist, close to the abdomen, to collect linear acceleration in the vertical direction and yaw angle data at a sampling rate of 50 Hz. For the purpose of replicating experiments, two specific sites were chosen:

1. For horizontal walking path, the pedestrian walked at a constant speed in the following order: starting point → C → B → A → D, covering a walking distance of approximately 150 meters.
2. For three-dimensional walking path, the pedestrian walked at a constant speed following this order: walking half a circle on the 4th floor → going downstairs → walking half a circle on the 3rd floor → going upstairs → walking back to the starting point on the 4th floor. The total covered walking distance is approximately 145 meters.

 doi:10.20944/preprints202402.1364.v1

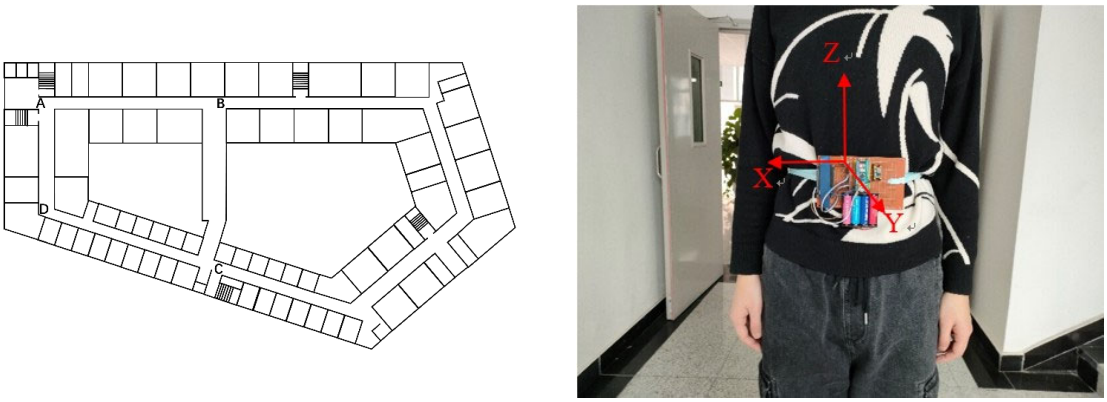

(**a**) (**b**)

Figure 8. Experimental design: (**a**) Schematic diagram of building plane structure; (**b**) Wearing method of inertial sensor.

The collected pedestrian walking three-dimensional path data were used as the testing set, while the sample data was used as the training set. The obtained classification results are presented in Table 2. Terrain features were deduced based on the motion patterns identified through pattern feature matching. The sequence observed was as follows: level ground → descent via stairs (to a lower floor) → level ground → ascent via stairs (to an upper floor) → level ground. This pattern aligns cohesively with the actual scenario.

Table 2. Walking data classification results. 'U ' represents going upstairs, ' H ' represents walking horizontally, and ' D ' represents going downstairs.

Walking data	L_1	L_2	L_3	L_4	L_5	L_6	L_7	L_8	L_9
Recognition result	H	D	D	H	H	U	U	H	H

After pedestrian motion pattern recognition and position matching calibration, the inertial navigation positioning calibration results were acquired. The calibrated indoor walking path is shown in Figure 9. Through terrain feature matching, the stair path underwent stair feature point coordinate calibration, while the horizontal walking path underwent calibration of the corridor turning point coordinate, step length, and yaw. The results shown in Figure 9(b) can verify the feasibility of the proposed method in 3D positioning. The path trajectory after terrain feature matching calibration closely corresponds to the actual walking path.

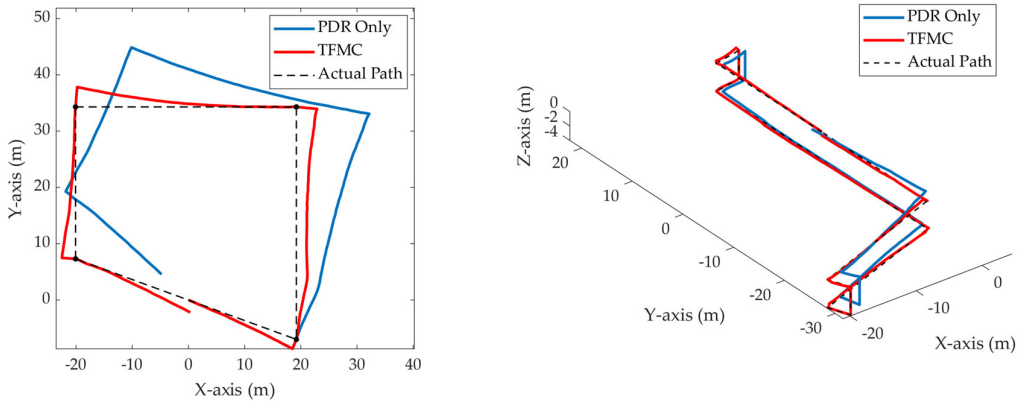

(**a**) (**b**)

 doi:10.20944/preprints202402.1364.v1

Figure 9. The path diagram before and after the TFMC; (a) Calibration of the corner feature points of the horizontal corridor; (b) Calibration of stair entrance and corridor corner feature points of the three-dimensional path.

Figure 10 shows the variation of the positioning error with the walking distance before and after the TFMC. Before the TFMC, the PDR positioning error noticeably accumulates with time. The positioning error is significantly reduced at each feature point by using the TFMC. The improvement in positioning performance is attributed to the combined effect of coordinate calibration, step length calibration, and yaw calibration for horizontal walking path, along with coordinate calibration for walking on stair paths.

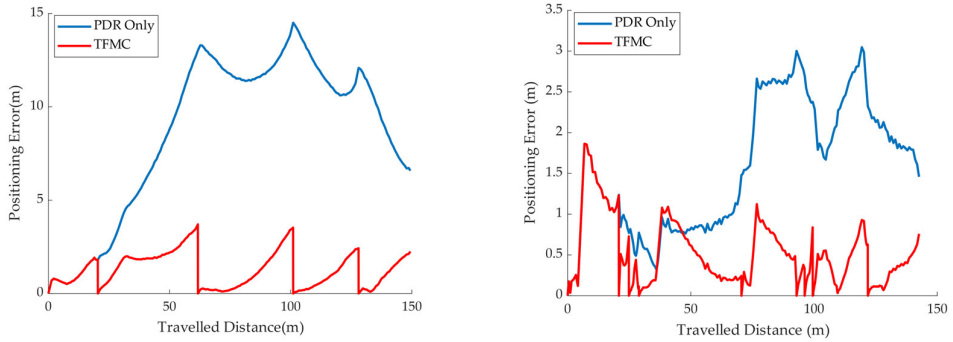

(**a**) (**b**)

Figure 10. The comparison map of positioning error before and after the TFMC; (a) Calibration of the corner feature points of the horizontal corridor; (b) Calibration of stair entrance and corridor corner feature points of the three-dimensional path.

In Figure 11, the cumulative distribution function (CDF) of positioning error is presented for cases where single calibration measurement is omitted. It shows that the TFMC method keeps 90 % of the 2D positioning error within 2.5 m, while 90 % of the 3D positioning error is kept within 1 m. And it is notable that yaw calibration yields the most influential improvement in positioning performance, while the improvements brought about by coordinate calibration and step length calibration are relatively modest and have similar effects.

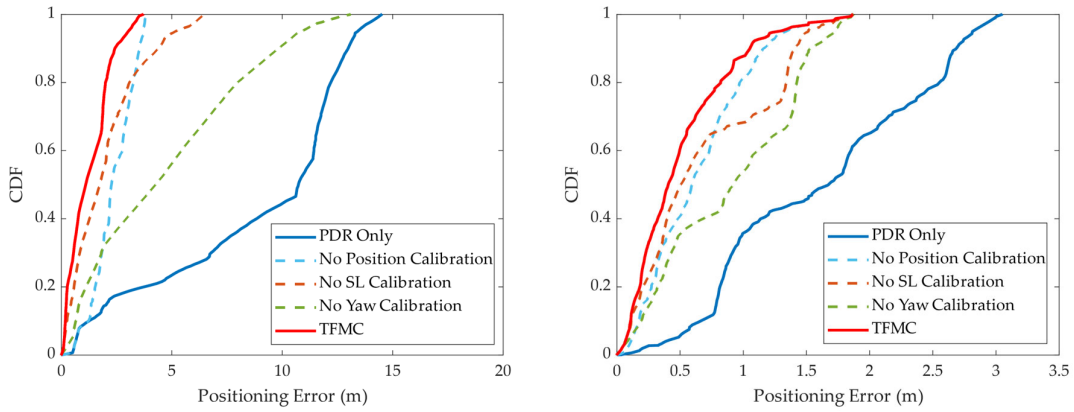

(**a**) (**b**)

Figure 11. The influence of position calibration, SL calibration and yaw calibration on positioning performance; (a) Horizontal path; (b) Three-dimensional path.

Table 3 summarizes the average positioning error, maximum positioning error, and root mean square error (RMSE) after terrain feature matching calibration. The result shows that the TFMC method can significantly reduce the average error of PDR positioning from 6.60 m to 1.83 m, resulting

 doi:10.20944/preprints202402.1364.v1

in higher positioning accuracy. Compared with the work of Ref. [23], our proposed method further achieves complete 3D positioning under the premise of ensuring similar positioning accuracy.

Table 3. Comparison of positioning errors after the TFMC.

Positioning error	PDR Only	TFMC
Average error (m)	6.60	1.83
Maximum error (m)	12.15	4.69
RMSE (m)	7.45	2.17

5. Conclusions

In this work, an indoor 3D positioning algorithm using Terrain Feature Matching Calibration (TFMC) is proposed. The proposed method contains motion pattern identification and PDR error elimination. Motion pattern identification matches pedestrian moving patterns to the terrain. Stair entrances were matched with the changed points of horizontal walking to the stairs, and corners of the corridor were matched with the turning points of pedestrian. PDR error elimination is achieved by performing the calibration. Experimental results show that the accuracy of motion pattern identification is over 99%, and the average positioning error decreases from 6.60 meters to 1.83 meters, thus calibrating pedestrian 3D walking trajectory accurately. Due to its sole reliance on inertial sensors without the necessity for additional sensors, the proposed method ensures both convenience and cost-effectiveness, making it a promising choice for indoor positioning in various LBS applications.

Author Contributions: Conceptualization, X.C. and Y.H.; methodology, X.C.; software, X.C. and Y.X.; validation, Y.X., X.C. and Y.H.; formal analysis, X.C.; investigation, X.C.; resources, X.C.; data curation, Y.H. and X.C.; writing—original draft preparation, Y.X., Z.Z. and X.C.; writing—review and editing, Y.X., Z.Z., Q.W. and X.C.; visualization, X.C.; supervision, Z.C.; project administration, Z.C.; funding acquisition, Z.C. All authors have read and agreed to the published version of the manuscript.

Funding: This research was supported by the Municipal Government of Quzhou under Grant No. 2022D004.

Data Availability Statement: No new data were created or analyzed in this study. Data sharing is not applicable to this article.

Conflicts of Interest: The authors declare no conflict of interest.

References

1. Zhang, H.; Hu, J.; Zhang, H.; Di, B.; Bian, K.; Han, Z.; Song, L. MetaRadar: Indoor Localization by Reconfigurable Metamaterials. *Ieee Transactions on Mobile Computing* **2022**, *21*, 2895-2908, doi:10.1109/tmc.2020.3044603.
2. Bastos, A.S.; Vieira, V.; ApolinArio, A.L. Indoor location systems in emergency scenarios: A Survey. In Proceedings of the Proceedings of the annual conference on Brazilian Symposium on Information Systems: Information Systems: A Computer Socio-Technical Perspective - Volume 1, Goiania, Goias, Brazil, 2015; pp. 251–258.
3. Shipkovenski, G.; Kalushkov, T.; Petkov, E.; Angelov, V.; Ieee. A Beacon-Based Indoor Positioning System for Location Tracking of Patients in Hospital. In Proceedings of the 2nd International Congress on Human-Computer Interaction, Optimization and Robotic Applications (HORA), Turkey, 2020 Jun 26-27, 2020; pp. 514-519.
4. Farahsari, P.S.; Farahzadi, A.; Rezazadeh, J.; Bagheri, A. A Survey on Indoor Positioning Systems for IoT-Based Applications. *Ieee Internet of Things Journal* **2022**, *9*, 7680-7699, doi:10.1109/jiot.2022.3149048.
5. Yuan, C.; Lai, J.Z.; Lyu, P.; Shi, P.; Zhao, W.; Huang, K. A Novel Fault-Tolerant Navigation and Positioning Method with Stereo-Camera/Micro Electro Mechanical Systems Inertial Measurement Unit (MEMS-IMU) in Hostile Environment. *Micromachines* **2018**, *9*, doi:10.3390/mi9120626.
6. Lin, T.Y.; Zhang, Z.Y.; Tian, Z.S.; Zhou, M. Low-Cost BD/MEMS Tightly-Coupled Pedestrian Navigation Algorithm. *Micromachines* **2016**, *7*, doi:10.3390/mi7050091.
7. Xiao, Z.L.; Wen, H.K.; Markham, A.; Trigoni, N.; Ieee. Robust pedestrian dead reckoning (R-PDR) for arbitrary mobile device placement. In Proceedings of the International Conference on Indoor Positioning and Indoor Navigation (IPIN), Minist Land Infrastructure & Transport, Buan, SOUTH KOREA, Oct 27-30, 2014; pp. 187-196.

8. Wang, Y.; Zhao, H. Improved Smartphone-Based Indoor Pedestrian Dead Reckoning Assisted by Visible Light Positioning. *Ieee Sensors Journal* **2019**, *19*, 2902-2908, doi:10.1109/jsen.2018.2888493.
9. He, K.; Zhang, Y.Y.; Zhu, Y.P.; Xia, W.W.; Jia, Z.Y.; Shen, L.F.; Ieee. A Hybrid Indoor Positioning System Based on UWB and Inertial Navigation. In Proceedings of the 7th IEEE International Conference on Wireless Communications and Signal Processing (WCSP), Nanjing, PEOPLES R CHINA, Oct 15-17, 2015.
10. Du, X.Q.; Liao, X.W.; Liu, M.M.; Gao, Z.Z. CRCLoc: A Crowdsourcing-Based Radio Map Construction Method for WiFi Fingerprinting Localization. *Ieee Internet of Things Journal* **2021**, *9*, 12364-12377, doi:10.1109/jiot.2021.3135700.
11. Koo, B.; Lee, S.; Lee, M.; Lee, D.; Lee, S.; Kim, S.; Ieee. PDR/Fingerprinting Fusion Indoor Location Tracking Using RSS Recovery and Clustering. In Proceedings of the International Conference on Indoor Positioning and Indoor Navigation (IPIN), Minist Land Infrastructure & Transport, Buan, SOUTH KOREA, Oct 27-30, 2014; pp. 699-704.
12. Wang, Q.; Luo, H.; Xiong, H.; Men, A.; Zhao, F.; Xia, M.; Ou, C. Pedestrian Dead Reckoning Based on Walking Pattern Recognition and Online Magnetic Fingerprint Trajectory Calibration. *Ieee Internet of Things Journal* **2021**, *8*, 2011-2026, doi:10.1109/jiot.2020.3016146.
13. Zhao, T.Y.; Ahamed, M.J. Pseudo-Zero Velocity Re-Detection Double Threshold Zero-Velocity Update (ZUPT) for Inertial Sensor-Based Pedestrian Navigation. *Ieee Sensors Journal* **2021**, *21*, 13772-13785, doi:10.1109/jsen.2021.3070144.
14. Wei, R.; Xu, H.; Yang, M.; Yu, X.; Xiao, Z.; Yan, B. Real-Time Pedestrian Tracking Terminal Based on Adaptive Zero Velocity Update. *Sensors* **2021**, *21*, doi:10.3390/s21113808.
15. Yu, N.; Li, Y.; Ma, X.; Wu, Y.; Feng, R. Comparison of Pedestrian Tracking Methods Based on Foot- and Waist-Mounted Inertial Sensors and Handheld Smartphones. *Ieee Sensors Journal* **2019**, *19*, 8160-8173, doi:10.1109/jsen.2019.2919721.
16. Hajati, N.; Rezaeizadeh, A. A Wearable Pedestrian Localization and Gait Identification System Using Kalman Filtered Inertial Data. *Ieee Transactions on Instrumentation and Measurement* **2021**, *70*, doi:10.1109/tim.2021.3073440.
17. Li, H.; Liu, Y.; Zhang, L.Q.; Wang, H. Magnetic Matching-Aided Indoor Localization System Based on a Waist-Mounted Self-Contained Sensor Array. *Journal of Sensors* **2022**, *2022*, doi:10.1155/2022/1710907.
18. Shi, J.; Ren, M.; Wang, P.; Meng, J. Research on PF-SLAM Indoor Pedestrian Localization Algorithm Based on Feature Point Map. *Micromachines* **2018**, *9*, doi:10.3390/mi9060267.
19. Gu, F.; Valaee, S.; Khoshelham, K.; Shang, J.; Zhang, R. Landmark Graph-Based Indoor Localization. *IEEE Internet of Things Journal* **2020**, *7*, 8343-8355, doi:10.1109/JIOT.2020.2989501.
20. Ghaoui, M.A.; Vincke, B.; Reynaud, R. Human Motion Likelihood Representation Map-Aided PDR Particle Filter. *Ieee Sensors Journal* **2023**, *23*, 484-494, doi:10.1109/jsen.2022.3222639.
21. Yang, W.; Xiu, C.D.; Zhang, J.M.; Yang, D.K. A Novel 3D Pedestrian Navigation Method for a Multiple Sensors-Based Foot-Mounted Inertial System. *Sensors* **2017**, *17*, doi:10.3390/s17112695.
22. Zhao, Y.L.; Liang, J.Q.; Sha, X.P.; Yu, J.N.; Duan, H.J.; Shi, G.Y.; Li, W.J. Estimation of Pedestrian Altitude Inside a Multi-Story Building Using an Integrated Micro-IMU and Barometer Device. *Ieee Access* **2019**, *7*, 84680-84689, doi:10.1109/access.2019.2924664.
23. Xie, D.P.; Jiang, J.G.; Yan, P.H.; Wu, J.J.; Li, Y.Y.; Yu, Z.Y. A Novel Three-Dimensional Positioning Method for Foot-Mounted Pedestrian Navigation System Using Low-Cost Inertial Sensor. *Electronics* **2023**, *12*, doi:10.3390/electronics12040845.
24. Wang, X.; Jiang, M.X.; Guo, Z.W.; Hu, N.J.; Sun, Z.W.; Liu, J. An Indoor Positioning Method for Smartphones Using Landmarks and PDR. *Sensors* **2016**, *16*, doi:10.3390/s16122135.
25. Xia, M.; Shi, C. Autonomous Pedestrian Altitude Estimation Inside a Multi-Story Building Assisted by Motion Recognition. *Ieee Access* **2020**, *8*, 104718-104727, doi:10.1109/access.2020.3000313.
26. Elhoushi, M.; Georgy, J.; Noureldin, A.; Korenberg, M.J. Motion Mode Recognition for Indoor Pedestrian Navigation Using Portable Devices. *Ieee Transactions on Instrumentation and Measurement* **2016**, *65*, 208-221, doi:10.1109/tim.2015.2477159.
27. Fang, Q.; Xu, X.; Wang, X.T.; Zeng, Y.J. Target-driven visual navigation in indoor scenes using reinforcement learning and imitation learning. *Caai Transactions on Intelligence Technology* **2022**, *7*, 167-176, doi:10.1049/cit2.12043.
28. Xia, H.; Zuo, J.B.; Liu, S.; Qiao, Y.Y. Indoor Localization on Smartphones Using Built-In Sensors and Map Constraints. *Ieee Transactions on Instrumentation and Measurement* **2019**, *68*, 1189-1198, doi:10.1109/tim.2018.2863478.
29. Khedr, M.; El-Sheimy, N. A Smartphone Step Counter Using IMU and Magnetometer for Navigation and Health Monitoring Applications. *Sensors* **2017**, *17*, doi:10.3390/s17112573.
30. Weinberg, H. Using the ADXL202 in pedometer and personal navigation applications.
31. Jang, B.; Kim, H.; Kim, J.W. Survey of Landmark-based Indoor Positioning Technologies. *Information Fusion* **2023**, *89*, 166-188, doi:10.1016/j.inffus.2022.08.013.

 doi:10.20944/preprints202402.1364.v1

32. He, S.N.; Chan, S.H.G. Wi-Fi Fingerprint-Based Indoor Positioning: Recent Advances and Comparisons. *Ieee Communications Surveys and Tutorials* **2016**, *18*, 466-490, doi:10.1109/comst.2015.2464084.